

# Main Manuscript for

## Direct observation of an incommensurate two-dimensional checkerboard charge density wave in the superconductor $\text{Ta}_4\text{Pd}_3\text{Te}_{16}$

S. J. Kuhn<sup>a,1</sup>, Zhenzhong Shi<sup>a,1</sup>, F. Flicker<sup>b</sup>, T. Helm<sup>c</sup>, J. Lee<sup>d</sup>, William Steinhardt<sup>a</sup>, Sachith Dissanayake<sup>a</sup>, D. Graf<sup>e</sup>, J. Ruff<sup>d</sup>, G. Fabbris<sup>f</sup>, D. Haskel<sup>f</sup>, and S. Haravifard<sup>a,g,2</sup>.

<sup>a</sup>Department of Physics, Duke University, Durham, NC 27708, USA; <sup>b</sup>Rudolph Peierls Centre for Theoretical Physics, University of Oxford, Department of Physics, Clarendon Laboratory, Parks Road, Oxford OX1 3PU, UK; <sup>c</sup>Max Planck Institute for Chemical Physics of Solids, Dresden, Germany; <sup>d</sup>Cornell High Energy Synchrotron Source, Cornell University, Ithaca, NY 14853, USA; <sup>e</sup>National High Magnetic Field Laboratory, Florida State University, Tallahassee, FL 32310, USA; <sup>f</sup>Advanced Photon Source, Argonne National Laboratory, Argonne, IL 60439, USA; <sup>g</sup>Department of Mechanical Engineering & Materials Science, Duke University, Durham, NC 27708, USA

<sup>1</sup> S.K. and Z.S. contributed equally to this work

<sup>2</sup> To whom correspondence should be addressed: S. Haravifard

Email: [haravifard@phy.duke.edu](mailto:haravifard@phy.duke.edu)

### Classification

PHYSICAL SCIENCES: Physics.

### Keywords

charge density wave | superconductivity | synchrotron X-ray diffraction | quantum oscillation | high pressure

### Author Contributions

S.H. designed and supervised research; T.H. grew the sample; S.K., J.L., J.R., D.H., and S.H. conducted X-ray diffraction study at ambient pressure; Z.S., W.S., S.D., G.F., D.H., and S.H. conducted X-ray diffraction study at high pressure; Z.S., D.G., and S.H. conducted quantum oscillation measurements; Z.S., F.F., and S.H. analyzed the data and wrote the paper.

The authors declare no conflict of interest.

### This PDF file includes:

Main Text  
Figures 1 to 6

### Abstract

We report the observation of a highly unusual incommensurate two-dimensional checkerboard charge density wave (CDW) in the superconductor  $\text{Ta}_4\text{Pd}_3\text{Te}_{16}$ , using synchrotron X-ray diffraction. We observe two CDW wavevectors, related by a crystal symmetry, developing below 16 K at ambient pressure. The wavevectors, which remain incommensurate at all observed temperatures, lie neither within the quasi-one-dimensional (Q1D) chains nor the Q2D planes in which the chains reside in this monoclinic crystal structure. The bulk CDW wavevectors are shown to reconcile previous scanning tunneling microscopy and transport studies. We also conducted de Haas-van Alphen (dHvA) quantum oscillation measurements and found no evidence of Fermi surface reconstruction through the CDW transition, suggesting a very subtle gap opening. We determine

the temperature-pressure ( $T$ - $P$ ) phase diagram, and find the superconductivity (SC) dome to be centered at the pressure where the CDW instability vanishes, suggesting that the SC in  $\text{Ta}_4\text{Pd}_3\text{Te}_{16}$  could have its origin in a CDW quantum critical point, reminiscent of the observations in many unconventional superconductors. With a thorough comparison to other CDW materials, we conclude that  $\text{Ta}_4\text{Pd}_3\text{Te}_{16}$  is a unique CDW system that features a mixed character of Q1D, Q2D, and 3D.

## Significance Statement

Charge density waves (CDWs) are an electronic instability originally proposed in the 1930s in a toy model of an ideal one-dimensional (1D) system. They have been experimentally identified in many low-dimensional systems, and are often found in close proximity to other electronic instabilities such as superconductivity (SC). The origin of CDWs and their interplay with SC in various materials is a central topic in condensed matter physics. Here we study the CDW in  $\text{Ta}_4\text{Pd}_3\text{Te}_{16}$ . Previously considered a Q1D superconductor, our results reveal an unexpected checkerboard CDW structure. We identify this material as a unique example of a CDW system with a hybrid character of Q1D, Q2D, and 3D.

## Main Text

### Introduction

Materials with unconventional superconductivity (SC) often have complex phase diagrams where SC is proximal to (or coexists with) competing orders, a complete description of which remains one of the greatest challenges in condensed matter physics (1–3). One important competing order is the charge density wave (CDW) in its various forms, such as those found in cuprates (4–6), binary chalcogenides, and trichalcogenides (7–10), where SC and CDWs coexist in certain parts of the phase diagram. Understanding the mechanism of the CDW order is therefore a crucial step in unlocking its relation with other collective ground states including SC (9–11). Despite decades of extensive research, the subject remains active as the conventional Peierls-like weak-coupling picture (12) proves to be insufficient in many cases (13).

Quasi-one-dimensional (Q1D) systems such as the transition metal trichalcogenide compounds are generically expected to be unstable to the development of CDWs via the Peierls instability, i.e. Fermi surface (FS) nesting (FSN) (14). While CDWs have been seen in Q2D systems such as the transition metal dichalcogenides, FSN is not the natural explanation in dimensions higher than one. A single wavevector will always nest the two points of the FS onto one another in 1D; in 2D and 3D a special shape of FS would be required to match large portions of the FS onto itself. Instead, a checkerboard two-dimensional (2D) CDW, present in materials such as  $\text{NbSe}_2$ , often has its origin in a more complicated picture involving the momentum and orbital dependence of the electron-phonon coupling matrix (15, 16). While much progress has already been made by studying these prototypical CDW materials, new systems on which the recent theoretical development can be tested are urgently needed.

Featuring three chains of  $\text{PdTe}_2$ ,  $\text{TaTe}_3$ , and  $\text{Ta}_2\text{Te}_4$  along its  $\mathbf{b}$ -axis, aligned into planes perpendicular to  $\mathbf{c}$ , the monoclinic crystalline structure of  $\text{Ta}_4\text{Pd}_3\text{Te}_{16}$  [shown in Fig. 1(a)] is reminiscent of those of trichalcogenide compounds such as  $\text{ZrSe}_3$ ,  $\text{TaSe}_3$ ,  $\text{NbSe}_3$ , and  $\text{TaS}_3$  (17). However, transport measurements on  $\text{Ta}_4\text{Pd}_3\text{Te}_{16}$  indicate resistivity ratios along the  $a^* : b : c$  directions of 4 : 1 : 13 at room temperature, evolving to 10 : 1 : 20 just above the superconducting

transition of  $T_c = 4.6$  K (18). The ratios suggest that the material is better thought of as having a character of mixed dimensionality: Q1D (along **b**), Q2D (perpendicular to **c**), and 3D.

Previous studies of  $\text{Ta}_4\text{Pd}_3\text{Te}_{16}$  have revealed an anisotropic SC ground state (19, 20). Upon application of pressure, a dome-shaped SC phase with maximum  $T_c \sim 6$  K at 0.2 GPa was discovered (21, 22). Some evidence suggests that the SC order parameter in  $\text{Ta}_4\text{Pd}_3\text{Te}_{16}$  might have a d-wave symmetry and thus an unconventional origin (19, 21, 23). Others have argued that the experimental findings may be explained by the more conventional s-wave SC order parameter and the multi-band nature of the compound (24, 25), consistent with band structure calculations (26). While phase-sensitive measurements may be needed to eventually reveal the pairing symmetry, the multiband SC in  $\text{Ta}_4\text{Pd}_3\text{Te}_{16}$  is also interesting because of some evidence of its proximity to a CDW phase (18, 24-27). The NMR/NQR measurements (25) and thermodynamic measurements (18) seem to suggest a CDW transition temperature of around 20 K, while Raman scattering measurements support the emergence of CDW fluctuations below 140 K  $\sim$  200 K (27). Additionally, STM measurements have shown period-4 commensurate CDW-like stripes along the **b**-axis that coexist with SC (24). However, the suggested wavevector is seemingly at odds with transport measurements, which reveal a resistivity anomaly primarily along the **a**\*-direction (18). Therefore, a direct measurement of the bulk CDW in  $\text{Ta}_4\text{Pd}_3\text{Te}_{16}$  is critical for reconciling these experimental results and understanding the interplay of SC and CDW in this material.

In this paper, we report a direct observation of an incommensurate bulk CDW in  $\text{Ta}_4\text{Pd}_3\text{Te}_{16}$  using synchrotron X-ray diffraction, at both ambient and high pressure. We establish the temperature-pressure ( $T$ - $P$ ) phase diagram, which reveals that the transition temperature of the CDW ( $T_{\text{CDW}}$ ) is  $\sim 16$  K at ambient  $P$ , and is quickly suppressed with increasing  $P$ , becoming undetectable where the SC transition temperature  $T_c$  reaches its maximum. Our de Haas-van Alphen (dHvA) oscillation measurements do not show any sign of FS reconstruction through the CDW transition, consistent with an earlier report (18). The observed CDW has a checkerboard pattern in real space, which resembles more closely the checkerboard CDW in quasi-2D systems such as  $\text{NbSe}_2$  (10) rather than those in typical Q1D systems such as  $\text{NbSe}_3$ , where multiple CDWs, if they exist, are typically unidirectional and independent (9). However, unlike the CDWs seen in Q2D systems, the CDW in  $\text{Ta}_4\text{Pd}_3\text{Te}_{16}$  does not lie within the Q2D planes. It would seem that the CDW in  $\text{Ta}_4\text{Pd}_3\text{Te}_{16}$  - a rare example of an incommensurate checkerboard CDW which coexists with SC - is its own beast.

## Results

**dHvA Quantum Oscillation.** In CDW systems where the FS is reconstructed as the bands backfold onto one another and translated through the CDW wavevector, this change in FS topology can often be detected in quantum oscillation (QO) measurements, if the FS is closed. We have therefore conducted dHvA oscillation measurements (Materials and Methods), and the background-subtracted results are shown in Fig. 1(b). Here, the fast Fourier transform taken for the field window of 5.4 T and 18 T reveals two frequencies  $F_1$  and  $F_2$  [Fig. 1(c)]. The fitting of the Lifshitz-Kosevich temperature damping factor  $R_T = (K\mu T/B)/\sinh(K\mu T/B)$  results in an effective mass of  $\mu_{F1} = (0.108 \pm 0.005)m_e$  and  $\mu_{F2} = (0.127 \pm 0.008)m_e$ , where  $m_e$  is the bare electron mass and  $K = 14.7$  T/K. The results are in rough agreement with the lowest two frequencies reported in Ref. (18), and in both cases, no FS reconstruction is observed as  $T$  is tuned through  $T_{\text{CDW}} \sim 16$  K.

To explain the observed QO results (18) a scenario was postulated in which an incommensurate CDW, already appearing at higher  $T$ , undergoes an incommensurate-to-commensurate lock-in transition at  $\sim 20$  K. However, as we show below, our X-ray results reveal an incommensurate CDW at  $T$  down to 3.5 K. The QO results therefore cannot be explained by a lock-in transition at  $T_{\text{CDW}}$ . Instead, this aspect of the CDW seems similar to that of NbSe<sub>2</sub>, where the CDW gap opens only at select points on one band of the multi-orbital FS and the change in the topology of the FS might be very subtle (28).

**Ambient-pressure X-ray Diffraction.** We obtained our most direct evidence of a checkerboard CDW in Ta<sub>4</sub>Pd<sub>3</sub>Te<sub>16</sub> using ambient-pressure X-ray diffraction (Materials and Methods), which provides an unambiguous identification of the bulk CDW and its wavevector. Using a high-dynamic-range area detector, we scanned wide areas across multiple Brillouin zones in many directions, including along the CDW wavevector [0 0.25 0] suggested by the previous STM study (24). However, our X-ray scans did not reveal any CDW peak along this direction. Instead, we identified two peaks with wavevectors Q1 = [-0.2 0.21 -0.3] and Q2 = [0.2 0.21 0.3] in all the Brillouin zones within our detection range. For example, in figure 2(a), which shows a 2D cut of the diffraction pattern along the **H** and **L** directions at  $K = 4.21$ , a superlattice with Q1 and Q2 wavevectors is clearly observed. We made the same observation at  $K = 2.21$ . The Q1 and Q2 wavevectors are related by a 180° rotation about the **b**-axis. Together they constitute commensurate patterns along the **H** and **L** (or **a\*** and **c\***) directions. We repeated the measurements at different temperatures from 3.5 K up to 30 K. Figure 2(b) shows the line-cuts and their Lorentzian fits along the  $K$  direction for the Q1 CDW near the (-1 4 1) Bragg peak at selected temperatures. At 3.5 K, the integrated intensity of the CDW peak is  $\sim 10^{-3}$  the strength of that at the nearby Bragg peak. Note that such a clear CDW peak below  $T_c \sim 4.6$  K (Ref. (17)) reveals a coexistence of the CDW and SC, consistent with the STM result (24). With increasing  $T$ , the Q1 CDW peak intensity first increases and peaks at  $\sim 7$  K, then diminishes and becomes undetectable at 16 K. A slight shift in the peak position with increasing  $T$  is also seen. Using the  $\mathbf{q}_k$  line cuts from all measured temperatures including those shown in Fig. 2(b), a color contour plot of the Q1 CDW peak intensity is shown [Fig. 2(c)], where a transition temperature of  $T_{\text{CDW}} = 16$  K is apparent. Our results are consistent with the  $\sim 20$  K transition temperature inferred from NMR/NQR measurements (25) and transport measurements (25). We do not see any evidence of a static CDW above  $T_{\text{CDW}} = 16$  K, though our measurements cannot rule out the possibility of fluctuating CDW order at these higher temperatures. The signatures of phonon anomalies at higher  $T$  (27) might therefore be attributed to a pseudogap phase, similar to that in NbSe<sub>2</sub> (29).

**High-pressure X-ray Diffraction.** To confirm our observations at ambient pressure, and to further explore the  $T$ - $P$  phase diagram, we also conducted X-ray diffraction under pressure at a different synchrotron source (APS, see Materials and Methods). At  $T = 4.3$  K and  $P = 0.2$  GPa, we again observed the Q1 and Q2 CDWs near the (3 -1 0) Bragg peak, as shown in Fig. 3(a). The ratio of the integrated intensity of the CDW peak and the nearby Bragg peak is again  $\sim 10^{-3}$ , in good agreement with our ambient pressure results. The intensities of the two CDWs are comparable within error, consistent with the picture of one checkerboard CDW. The temperature dependence of the  $\mathbf{q}_k$  line cuts are measured for the Q2 CDW at  $P = 0.2$  GPa. The results as seen in Fig. 3(b) clearly show that the peak intensity is quickly suppressed with increasing  $T$ , and becomes undetectable at 12 K. Moreover, our experiments at higher pressure (0.35 GPa) do not show any CDW peaks, suggesting a drastic suppression of CDW by pressure. Earlier studies (21, 22) have revealed a SC dome with maximum  $T_c$  at  $0.2 \sim 0.3$  GPa. Our results are consistent with the picture

in which the CDW competes with the SC, in a manner reminiscent of many unconventional superconductors (2).

**Temperature and pressure dependence of the CDW.** We have also compared the CDW peak properties at  $P = 0$  and 0.2 GPa. The results of the integrated peak intensity, the peak center along  $\mathbf{q}_k$ , and the full width at half maximum (FWHM) from the Lorentzian fits, are shown in Figs. 4 (a-c), respectively. The CDW peak intensity is suppressed below  $T_c$  and with increasing  $P$ , due to its competition with SC. The temperature dependence of the CDW peak position along  $\mathbf{q}_k$ , as shown in Fig.4(b), shows some unexpected properties. At ambient pressure the CDW peak center along  $\mathbf{q}_k$  shifts towards a commensurate value 0.2 (a real-space periodicity of 5) with decreasing  $T$ , but saturates before locking into a commensurate value. The peak also shifts further away from  $\mathbf{q}_k = 0.2$  under pressure. Therefore, it appears that the CDW remains incommensurate along  $\mathbf{q}_k$  down to the lowest measured temperatures. Typically, one expects the CDW wavevector to evolve continuously with temperature until abruptly jumping to a commensurate value, in a lock-in phase transition (11). Examples include Q1D TTF-TCNQ and Q2D TaSe<sub>2</sub>. However, many other materials show an evolution of the CDW wavevector without an eventual lock-in (9). Examples of this include Q1D NbSe<sub>3</sub> and TbTe<sub>3</sub> and Q2D NbSe<sub>2</sub>. Our observations indicate that TPT falls into this latter category.

The CDW wavevectors that we have identified with our X-ray measurements appear at first to be in contrast to the CDW found in a previous STM study (24), in which a period-4 commensurate CDW along the  $\mathbf{b}$ -axis was suggested. However, as we discuss below, our results for the bulk CDW are actually consistent with those from STM, which is only sensitive to a projection of the charge modulation onto the sample surface, i.e. the (-1 0 3) cleavage plane. This reconciles the apparently conflicting results from STM (24) and transport measurements (18).

The  $T$ -dependent FWHM at  $P = 0$  and 0.2 GPa are plotted in Fig. 4(c). The FWHM at low temperature is  $\sim 0.1$  r.l.u., suggesting a CDW correlation length  $\xi_{\text{CDW}} (= 2/\text{FWHM}) \sim 120 \text{ \AA}$  along  $\mathbf{q}_k$ . The width of the Bragg peak is resolution limited and two orders of magnitude smaller. A slight increase of FWHM to 0.15 r.l.u. is seen below  $T_c$  due to competition from SC. Near  $T_{\text{CDW}}$  the FWHM increases drastically and  $\xi_{\text{CDW}} \sim 30 \text{ \AA}$  close to the CDW wavelength along the  $\mathbf{b}$ -axis  $\lambda_b \sim 5b \sim 20 \text{ \AA}$ , signaling the melting of the static CDW at higher  $T$ .

**$T$ - $P$  phase diagram.** In Fig. 4(d) we establish a  $T$ - $P$  phase diagram using  $T_{\text{CDW}}(P)$  obtained from our X-ray measurements and  $T_c$  from Ref. (22). The pressure at which the CDW order vanishes matches that at which the SC dome is peaked. This behavior is reminiscent of many unconventional superconductors in which the SC dome appears centered at a quantum critical point (QCP) at which a competing order vanishes (2). It is tempting to speculate that the SC in Ta<sub>4</sub>Pd<sub>3</sub>Te<sub>16</sub> might also have an origin related to the QCP of a CDW instability. Our results therefore add to the debate over the SC mechanism in this system (19, 21, 23–25), and future investigations on the SC and CDW orders in Ta<sub>4</sub>Pd<sub>3</sub>Te<sub>16</sub> using techniques such as phase-sensitive measurements and angle-photoemission spectroscopy are highly desirable.

## Discussion

**CDW Structure in Ta<sub>4</sub>Pd<sub>3</sub>Te<sub>16</sub>.** Our results indicate a 2D checkerboard CDW defined by the two CDW wavevectors. The projection of the CDW into the  $\mathbf{a}$ - $\mathbf{c}$  plane has a period of 5 along  $\mathbf{a}$  and a period of 10/3 along  $\mathbf{c}$ . As there are 3 chains per unit cell along  $\mathbf{c}$ , the length of 10c/3 corresponds

to a period of 10 chains in this direction. Q1 and Q2 both project in the same way in the **a-c** plane. STM accesses the (-1 0 3) cleavage plane, containing the perpendicular vectors  $\mathbf{a}^*$  and  $\mathbf{b}$ . In the  $\mathbf{a}^*$  direction the crystal structure repeats every 49.8 Å, which we define to be  $a_{\perp}$ . The projection of the CDWs along  $\mathbf{a}^*$  give a period  $1.13a_{\perp}$  distortion. In the  $\mathbf{b}$  direction, both CDW wavevectors give a period  $b/0.21 \approx 4.76b$  distortion. While the periodicities seen by X-rays are therefore incommensurate in both the  $\mathbf{a}^*$  and  $\mathbf{b}$  directions, the resulting CDW patterns would be expected to lock into commensurate structures locally, with phase slips to allow for the globally incommensurate patterns (30, 31). This is expected both in the bulk and on the surface; however, surface effects could plausibly fully stabilize the commensurate CDW, removing the phase slips. The CDW would normally lock into a nearby rational period, with lower periods expected to be favored. STM would therefore be likely to see a CDW with period of either 4 or 5 along  $\mathbf{b}$ , and period 1 (i.e. no CDW) or 2 along  $\mathbf{a}^*$ . Carrying out the Fourier transform of the STM image given in Ref. (24), the resulting diffraction peaks can be indexed with  $\mathbf{a}^*_{\perp} \pm \mathbf{b}^*/4$ , where  $\mathbf{a}^*_{\perp}$  is a vector along  $\mathbf{a}^*$  of length  $2\pi/a_{\perp}$ . The surface CDW is therefore of period one along  $\mathbf{a}^*$  and four along  $\mathbf{b}$ , and is consistent with our X-ray measurements.

Our results also shed light on the resistivity anomaly observed in the transport study (18). At  $T_{\text{CDW}} \sim 16$  K, it was reported (18) that an increase of resistivity was observed along the  $\mathbf{a}^*$  direction, while far less significant increases were seen along the  $\mathbf{b}$  and  $\mathbf{c}$  directions. This is despite STM reporting a charge modulation along  $\mathbf{b}$ . Our X-ray results show a commensurate structure in the **a-c** plane, with a large component along  $\mathbf{a}^*$ . Therefore, a resistivity bump along that direction comes as no surprise. The CDW component along  $\mathbf{b}$  is incommensurate with the lattice (in the bulk of the crystal, if not along the surface), which could explain the lack of a resistivity feature associated with the CDW in this direction.

**Comparison with other CDW systems.** Our measurements and analysis thus reveal a 2D checkerboard CDW in  $\text{Ta}_4\text{Pd}_3\text{Te}_{16}$ . The material is often considered as Q1D, structurally similar to the transition metal trichalcogenides such as  $\text{NbSe}_3$ ,  $\text{NbS}_3$ ,  $\text{ZrSe}_3$ , and  $\text{TaSe}_3$ , each of which has a monoclinic phase formed from chains within planes and hosts multiple CDWs (9). The case of  $\text{NbSe}_3$  is representative of the class, and is the prototypical example of a Q1D Peierls CDW material. It hosts two CDWs with wavevectors  $Q1 = (0 \ 0.241 \ 0)$ ,  $Q2 = (1/2 \ 0.260 \ 1/2)$  (32). The Q2 CDW is known to develop at a higher temperature on the surface of the material than in the bulk, with the surface order believed to develop in a Kosterlitz-Thouless transition (33). STM sees a locally commensurate CDW structure on the surface, with periodic phase slips allowing for an incommensurate average wavevector (34). These facts align with our suggestions above regarding discrepancies between the surface and bulk probes of the CDW order in  $\text{Ta}_4\text{Pd}_3\text{Te}_{16}$ . However, unlike  $\text{Ta}_4\text{Pd}_3\text{Te}_{16}$ , the two CDWs in  $\text{NbSe}_3$  are not related by a lattice symmetry, and develop at different temperatures (35). They are therefore two independent CDWs, with independent order parameters, rather than a checkerboard CDW.

Another related class of Q1D CDW materials is the rare-earth tri-tellurides  $\text{RTe}_3$  ( $\text{R} = \text{Sm}, \text{Gd}, \text{Tb}, \text{Dy}, \text{Ho}, \text{Er}, \text{Tm}$ ). The crystal structure of these materials is weakly orthorhombic, but is very close to the monoclinic structure of  $\text{Ta}_4\text{Pd}_3\text{Te}_{16}$  (36). All of these compounds develop incommensurate CDWs with  $Q1 \approx 2c^*/7$ ; the heavier elements ( $\text{R} = \text{Dy}, \text{Ho}, \text{Er}, \text{Tm}$ ) also develop a second incommensurate CDW, with  $Q2 \approx a^*/3$ . However, as in the trichalcogenides, these two CDWs develop at different temperatures, and are not related by lattice symmetries.

The resistivity ratios of  $\text{Ta}_4\text{Pd}_3\text{Te}_{16}$  suggest that the material is better thought of not as Q1D but as a dimensional hybrid with Q1D chains within Q2D planes within a 3D material. DFT calculations confirm the existence of FS pockets of each dimensionality. For this reason a fairer comparison might be found with Q2D CDW materials such as the transition metal dichalcogenides  $2H\text{-NbSe}_2$ ,  $2H\text{-TaSe}_2$ , and  $1T\text{-TaS}_2$  (11, 37). The  $2H$  materials have a hexagonal crystal structure, and the  $1T$  a trigonal structure. In  $2H\text{-NbSe}_2$ , for example, a checker-board CDW develops within the hexagonal Q2D planes, with three incommensurate CDW wavevectors developing at the same temperature and related by the  $C_6$  lattice symmetry (38). However, in all these cases, the CDW which develops does so entirely within the Q2D planes. An exception is  $1T\text{-TiSe}_2$ , a Q2D TMDC which develops a three-dimensional commensurate  $2 \times 2 \times 2$  CDW, although even in this case the CDW fits to the Q2D planes, with order also between the planes (39).

Perhaps the closest relative of the CDW in  $\text{Ta}_4\text{Pd}_3\text{Te}_{16}$  is that in  $1T\text{-VSe}_2$ , a TMDC with a mixed Q2D and 3D character. This material develops a CDW with commensurate period-4 components within the Q2D planes, but an incommensurate component out-of-plane (40). The three CDW wavevectors are related by a  $C_3$  lattice symmetry, and develop at the same temperature. The incommensurate wavevector in  $\text{VSe}_2$  evolves with temperature but never locks into the lattice. The CDW has no corresponding FSN structure, as demonstrated by a lack of divergence in the electronic susceptibility (Lindhard response function) (41), and ARPES sees no obvious disruption of the FS as the CDW develops (42). Similarly,  $\text{Ta}_4\text{Pd}_3\text{Te}_{16}$  also has (a) a character of mixed dimensionality, (b) multiple CDWs developing at the same temperature, (c) CDW wavevectors that are commensurate along two lattice directions but incommensurate along the third (remaining incommensurate as temperature varies), (d) CDW wavevectors related by a lattice symmetry, and (e) no clear signatures of FS reconstruction as the CDW develops (see our dHvA measurements).

We made a simple estimate of the Lindhard function in  $\text{Ta}_4\text{Pd}_3\text{Te}_{16}$  using existing DFT data, and found no divergences (18, 26). This again suggests a more complicated origin of the CDW than simple FSN (13, 15). In general, FSN is not the natural assumption when CDWs are encountered in dimensions higher than one: while a single CDW wavevector can gap out the entire FS in 1D, in dimensions higher than one the wavevectors would need to connect large parts of the FS. It seems reasonable to surmise that the CDW mechanism in  $\text{Ta}_4\text{Pd}_3\text{Te}_{16}$  is the same as that in the other  $D > 1$  CDW systems: TMDCs  $2H\text{-NbSe}_2$  (16),  $2H\text{-TaSe}_2$  (43), and  $1T\text{-VSe}_2$  (41), in which the CDWs are known to originate from a structured electron-phonon coupling dependent on both the ingoing and outgoing electron momenta and the orbital content of the bands scattered between (28).

It has previously been argued that CDWs never truly develop by a Q1D Peierls-type mechanism (13, 16). From this point of view, all compounds with a purported low-dimensional character might more reasonably be thought of as dimensional hybrids, with  $\text{Ta}_4\text{Pd}_3\text{Te}_{16}$  simply being a particularly clear example. A consequence can be seen in the behavior of the CDW under pressure, and its interaction with SC states. As noted in Ref. (9), increasing pressure has the effect of increasing interchain (or interplane) coupling, which might have one of two opposite effects on  $T_{\text{CDW}}$  depending on how Q1D the system really is. In extreme Q1D systems,  $T_{\text{CDW}}$  is heavily suppressed by fluctuations to well below the value predicted by mean-field theory (44). The increased interchain coupling decreases the one-dimensional character of the system, suppressing these fluctuations, and increasing  $T_{\text{CDW}}$ . On the other hand, if  $T_{\text{CDW}}$  is not dictated by

Q1D fluctuations, the primary effect of the increased interchain coupling is to decrease the density of states at the Fermi level, suppressing  $T_{\text{CDW}}$ . At high enough pressure the CDW becomes unfeasible and is suppressed entirely. The phonon mode formerly suppressed by the CDW then becomes available to mediate SC, and an SC dome develops as a function of pressure.

In Fig. 5 and Fig. S1 we show the  $T$ - $P$  phase diagram of a number of materials including  $T_{\text{CDW}}$  (solid symbols) and  $T_c$  (empty symbols). This figure extends the results presented in Fig. 3.13 of Ref. (9). Amongst the materials reported as Q1D,  $(\text{TaSe}_4)_2\text{I}$  (45, 46) shows an initial increase in  $T_{\text{CDW}}$  with pressure, and monoclinic  $\text{TaS}_3$  appears to behave similarly, but the SC dome is not reached by the highest pressures of around 30 GPa. On the other hand,  $o\text{-TaS}_3$  (45, 46),  $\text{ZrTe}_3$ ,  $\text{GdTe}_3$ ,  $\text{TbTe}_3$ ,  $\text{DyTe}_3$  (47), and  $\text{NbSe}_3$  (45, 46) show a decrease in  $T_{\text{CDW}}$  with pressure. Despite the resistivity anisotropies of these materials indicating a Q1D nature, the  $T_{\text{CDW}}$  behavior fits more closely to 3D materials.

Since fluctuation effects would be expected to be smaller in Q2D than Q1D (while still significantly larger in Q2D than 3D), we might well expect all approximately-Q2D CDWs to be suppressed under pressure, again terminating in an SC dome. This behavior is confirmed in Fig. 5 and Fig. S1 for  $2H\text{-NbSe}_2$  (48),  $2H\text{-TaS}_2$  (49, 50),  $1T\text{-TaS}_2$  (51),  $1T\text{-TaSe}_2$  (52), and  $1T\text{-TiSe}_2$  (53). Recent work reports that the Q2D-3D hybrid  $1T\text{-VSe}_2$  shows an unexpected increase in  $T_{\text{CDW}}$  with pressure, followed by an abrupt suppression of the CDW and development of SC above around 15 GPa (54). However, these estimates are based on tracking the minimum in  $d\rho/dT$  from resistivity ( $\rho$ ) measurements, and the true relation between this quantity and the CDW state remains to be identified.

Alongside these data we present the results of our measurements of  $\text{Ta}_4\text{Pd}_3\text{Te}_{16}$ . We again see the suppression of the CDW with pressure, terminating in an SC dome. However, unlike all the CDW systems just discussed as featuring SC domes, the SC dome in  $\text{Ta}_4\text{Pd}_3\text{Te}_{16}$  reaches down to zero pressure. This is likely a consequence of  $T_{\text{CDW}}$  being low in the first place, meaning relatively little pressure is needed to suppress the CDW entirely. The reason for the exceptionally low  $T_{\text{CDW}}$  (the lowest of all discussed) is likely that the system is not really Q1D at all, but has a hybrid Q1D-Q2D-3D dimensionality. Moreover, a comparison between the CDW transition temperature ( $\sim 16$  K) and the energy gap ( $= 20 \sim 30$  meV) observed by STM (24) suggests that the CDW in  $\text{Ta}_4\text{Pd}_3\text{Te}_{16}$  is in the strong-coupling limit ( $3.52k_B T_c \gg 2\Delta$ ), similar to the charge order in  $\text{NbSe}_2$  (16) and cuprates (6). It is also interesting to point out that our observation is consistent with an early band structure study on rare-earth tellurides which suggests that a checkerboard state would occur with sufficiently low CDW transition temperature, while a unidirectional (stripe) CDW is favored with higher transition temperature (55).

Therefore, the behavior of  $\text{Ta}_4\text{Pd}_3\text{Te}_{16}$  resembles that seen in many unconventional superconductors such as the Q2D cuprates, where the SC dome also seems to center at QCPs of instabilities related to either CDW or other pseudogap orders (56). This brings forward an interesting speculation that the SC in  $\text{Ta}_4\text{Pd}_3\text{Te}_{16}$  might also have its origin in quantum fluctuations of a CDW instability. An incommensurate wavevector along  $\mathbf{b}$  down to our lowest-measured temperature might be a manifestation of the strong quantum fluctuation of the CDW order.  $\text{Ta}_4\text{Pd}_3\text{Te}_{16}$  seems to be an ideal platform on which to study the origin and the interplay of CDW order with a potential unconventional SC, beyond the conventional model systems.

## Materials and Methods

**Samples.** Our study was conducted on multiple single crystals of  $\text{Ta}_4\text{Pd}_3\text{Te}_{16}$  that were grown using a self-flux with excess tellurium at  $T$  up to  $1000^\circ\text{C}$ . High-resolution single-crystal X-ray diffraction confirmed the quality of the crystals and their orientations. The same batch of samples has been used in previous thermodynamic and transport studies (18).

**de Haas-van Alphen quantum oscillation.** The dHvA quantum oscillation measurements were performed in a  $^3\text{He}$  cryostat and an 18 T superconducting magnet at the National High Magnetic Field Laboratory (NHMFL) using piezo-resistive cantilevers and samples with typical dimensions  $\sim 60 \times 60 \times 30 \mu\text{m}^3$ .

**Synchrotron X-ray diffraction at ambient pressure.** The ambient-pressure high-dynamic-range diffraction maps were collected at the A2 beamline at Cornell High Energy Synchrotron Source (CHESS), using 19.37 keV X-rays and a fast photon-counting area detector. A needle-shaped single crystal sample was affixed at one end to a copper post, which was subsequently mounted in transmission geometry inside a closed-cycle cryostat with a base  $T$  of 3.5 K.

**Synchrotron X-ray diffraction at high pressure.** For high pressure measurements, single crystals of  $\text{Ta}_4\text{Pd}_3\text{Te}_{16}$  are cut into bar shapes with typical dimensions  $\sim 100 \times 60 \times 30 \mu\text{m}^3$  (length  $\times$  width  $\times$  thickness). Sample qualities were then checked using single-crystal X-ray diffraction, and the best samples were selected and loaded into a 800- $\mu\text{m}$ -culet diamond anvil cell using 4:1 Methanol:Ethanol as the hydrostatic pressure medium and a piece of polycrystalline gold as the manometer. In-situ pressure tuning was enabled by a helium gas membrane. The high-pressure experiments were conducted at the 4-ID-D beamline at the Advanced Photon Source (APS), using 19.5 keV X-rays, a six-circle diffraction stage, and a Sumitomo closed-cycle cryostat with a base  $T$  of 4 K.

## Acknowledgments

We acknowledge useful discussions with J. van Wezel and S. H. Simon, and experimental help from J. Stremper. This work is based upon research conducted at the Cornell High Energy Synchrotron Source (CHESS) which is supported by the National Science Foundation under award DMR-1332208. F. F. acknowledges support from the Astor Junior Research Fellowship of New College, Oxford. A portion of this work was performed at the National High Magnetic Field Laboratory, which is supported by National Science Foundation Cooperative Agreement No. DMR-1157490 and the State of Florida. Work at Duke University is funded by William M. Fairbank chair in physics endowment.

## References

1. A. M. Gabovich, A.I. Voitenko, and M. Ausloos, Charge- and spin-density waves in existing superconductors: competition between Cooper pairing and Peierls or excitonic instabilities. *Phys. Rep.* 367, 583 (2002).
2. M. R. Norman, The challenge of unconventional superconductivity. *Science* 332, 196 (2011).

3. E. Fradkin, S. A. Kivelson, and J. M. Tranquada, Colloquium: Theory of intertwined orders in high temperature superconductors. *Rev. Mod. Phys.* 87, 457 (2015).
4. T. Wu et al., Magnetic-field-induced charge-stripe order in the high-temperature superconductor  $\text{YBa}_2\text{Cu}_3\text{O}_y$ . *Nat. Commun.* 477, 191 (2011).
5. T. Wu et al., Incipient charge order observed by NMR in the normal state of  $\text{YBa}_2\text{Cu}_3\text{O}_y$ . *Nat. Commun.* 6, 6438 (2015).
6. R. Comin and A. Damascelli, Resonant X-Ray scattering studies of charge order in cuprates. *Annu. Rev. Condens. Matter Phys.* 7, 369 (2016).
7. D. E. Moncton, J. D. Axe, and F. J. DiSalvo, Study of superlattice formation in  $2H\text{-NbSe}_2$  and  $2H\text{-TaSe}_2$  by neutron scattering. *Phys. Rev. Lett.* 34, 734 (1975).
8. P. Monceau, N. P. Ong, A. M. Portis, A. Meerschaut, and J. Rouxel, Electric field breakdown of charge-density-wave-induced anomalies in  $\text{NbSe}_3$ . *Phys. Rev. Lett.* 37, 602 (1976).
9. P. Monceau, Electronic crystals: an experimental overview. *Adv. Phys.* 61, 325 (2012).
10. C.-W. Chen, J. Choe, and E. Morosan, Charge density waves in strongly correlated electron systems. *Rep. Prog. Phys.* 79, 084505 (2016).
11. Y. Feng et al., Itinerant density wave instabilities at classical and quantum critical points. *Nat. Phys.* 11, 865 (2015).
12. R. Peierls, *Quantum Theory of Solids*. Oxford University Press, London (1955).
13. M. D. Johannes and I. I. Mazin, Fermi surface nesting and the origin of charge density waves in metals. *Phys. Rev. B* 77, 165135 (2008).
14. G. Grüner, *The dynamics of charge-density waves*. *Rev. Mod. Phys.* 60, 1129 (1988).
15. X. Zhu, Y. Cao, J. Zhang, E. W. Plummer, and J. Guo, Proc. Classification of charge density waves based on their nature. *Natl. Acad. Sci. U.S.A.* 112, 2367 (2015).
16. F. Flicker and J. van Wezel, Charge order from orbital-dependent coupling evidenced by  $\text{NbSe}_2$ . *Nat. Commun.* 6, 7034 (2015).
17. W.-H. Jiao et al., Superconductivity in a layered  $\text{Ta}_4\text{Pd}_3\text{Te}_{16}$  with  $\text{PdTe}_2$  chains. *J. Am. Chem. Soc.* 136, 1284 (2014).
18. T. Helm et al., Thermodynamic anomaly above the superconducting critical temperature in the quasi-one-dimensional superconductor  $\text{Ta}_4\text{Pd}_3\text{Te}_{16}$ . *Phys. Rev. B* 95, 075121 (2017).
19. Z. Du et al., Anisotropic superconducting gap and elongated vortices with Caroli-De Gennes-Matricon states in the new superconductor  $\text{Ta}_4\text{Pd}_3\text{Te}_{16}$ . *Sci. Rep.* 5, 9408 (2015).
20. W.-H. Jiao et al., Superconductivity in  $\text{Ta}_3\text{Pd}_3\text{Te}_{14}$  with quasi-one-dimensional  $\text{PdTe}_3$  chains. *Sci. Rep.* 6, 21628 (2016).

21. J. Pan et al., Nodal superconductivity and superconducting dome in the layered superconductor  $\text{Ta}_4\text{Pd}_3\text{Te}_{16}$ . *Phys. Rev. B* 92, 180505(R) (2015).
22. N. H. Jo et al., Pressure induced change in the electronic state of  $\text{Ta}_4\text{Pd}_3\text{Te}_{16}$ . *Phys. Rev. B* 95, 134516 (2017).
23. G. Pang et al., Evidence for nodal superconductivity in a layered compound  $\text{Ta}_4\text{Pd}_3\text{Te}_{16}$ . *J. Phys.: Condens. Matter* 30, 055701 (2018).
24. Q. Fan et al., Scanning tunneling microscopy study of superconductivity, magnetic vortices, and possible charge-density wave in  $\text{Ta}_4\text{Pd}_3\text{Te}_{16}$ . *Phys. Rev. B* 91, 104506 (2015).
25. Z. Li, W. H. Jiao, G. H. Cao, and G.-q. Zheng, Charge fluctuations and nodeless superconductivity in quasi-one-dimensional  $\text{Ta}_4\text{Pd}_3\text{Te}_{16}$  revealed by  $^{125}\text{Te}$ -NMR and  $^{181}\text{Ta}$ -NQR. *Phys. Rev. B* 94, 174511 (2016).
26. D. J. Singh, Multiband superconductivity of  $\text{Ta}_4\text{Pd}_3\text{Te}_{16}$  from Te  $p$  states. *Phys. Rev. B* 90, 144501 (2014).
27. D. Chen et al., Raman scattering investigation of the quasi-one-dimensional superconductor  $\text{Ta}_4\text{Pd}_3\text{Te}_{16}$ . *J. Phys.: Condens. Matter* 27, 495701 (2015).
28. F. Flicker and J. van Wezel, Charge order in  $\text{NbSe}_2$ . *Phys. Rev. B* 94, 235135 (2016).
29. S. V. Borisenko, et al., Pseudogap and charge density waves in two dimensions. *Phys. Rev. Lett.* 100, 196402 (2008).
30. F. Flicker and Jasper van Wezel, Quasiperiodicity and 2D topology in 1D charge-ordered materials. *Europhysics Letters* 111, 37008 (2015).
31. W. L. McMillan, Theory of discommensurations and the commensurate-incommensurate charge-density-wave phase transition. *Phys. Rev. B* 14, 1496 (1976).
32. R. M. Fleming, D. E. Moncton, and D. B. McWhan, X-ray scattering and electric field studies of the sliding mode conductor  $\text{NbSe}_3$ . *Phys. Rev. B* 18, 5560 (1978).
33. C. Brun, Z. Z. Wang, P. Monceau, and S. Brazovskii, Surface Charge Density Wave Phase Transition in  $\text{NbSe}_3$ . *Phys. Rev. Lett.* 104 256403 (2010).
34. S. Brazovskii, C. Brun, Z. Z. Wang, and P. Monceau, Scanning-tunneling microscope imaging of single-electron solitons in a material with incommensurate charge-density waves. *Phys. Rev. Lett.* 108 096801 (2012).
35. J. Chaussy et al., Phase transitions in  $\text{NbSe}_3$ . *Solid State Commun.* 20, 759 (1976).
36. N. Ru et al., Effect of chemical pressure on the charge density wave transition in rare-earth tritellurides  $\text{RTe}_3$ . *Phys. Rev. B* 77, 035114 (2008).
37. B. Giambattista, C. Slough, W. McNairy, and R. Coleman, Scanning tunneling microscopy of atoms and charge-density waves in  $1T\text{-TaS}_2$ ,  $1T\text{-TaSe}_2$ , and  $1T\text{-VSe}_2$ . *Phys. Rev. B* 41, 10082 (1990).

38. J. A. Wilson, F. J. Di Salvo, and S. Mahajan, Charge-density waves in metallic, layered, transition-metal dichalcogenides. *Phys. Rev. Lett.* 32, 882-885 (1974).
39. A. Kogar et al., Signatures of exciton condensation in a transition metal dichalcogenide. *Science* 358, 1314-1317 (2017).
40. K. Tsutsumi, X-ray-diffraction study of the periodic lattice distortion associated with a charge-density wave in  $1T$ -VSe<sub>2</sub>. *Phys. Rev. B* 26, 5756 (1982).
41. J. Henke, J. Laverock, F. Flicker, and J. van Wezel, Charge order from structured coupling in VSe<sub>2</sub>. arXiv:1911.11112 (25 November 2019).
42. K. Terashima et al., Charge-density wave transition of  $1T$ -VSe<sub>2</sub> studied by angle-resolved photoemission spectroscopy. *Phys. Rev. B* 68, 155108 (2003).
43. W. Luckin, F. Flicker, and M. Mucha-Kruczynski, in preparation.
44. P. A. Lee, T. M. Rice, and P. W. Anderson, Fluctuation effects at a peierls transition. *Phys. Rev. Lett.* 31, 462 (1973).
45. M. Núñez-Regueiro et al., Superconductivity under pressure in linear chalcogenides. *Synthetic Metals* 55-57, 2653 (1993).
46. M. Núñez-Regueiro, J.-M. Mignot, and D. Castello, Superconductivity at High Pressure in NbSe<sub>3</sub>. *Europhys. Lett.* 18, 53 (1992).
47. D. A. Zocco et al., Pressure dependence of the charge-density-wave and superconducting states in GdTe<sub>3</sub>, TbTe<sub>3</sub>, and DyTe<sub>3</sub>. *Phys. Rev. B* 91, 205114 (2015).
48. M. Leroux et al., Strong anharmonicity induces quantum melting of charge density wave in  $2H$ -NbSe<sub>2</sub> under pressure. *Phys. Rev. B* 92, 140303(R) (2015).
49. R. Grasset et al., Pressure-Induced Collapse of the Charge Density Wave and Higgs Mode Visibility in  $2H$ -TaS<sub>2</sub>. *Phys. Rev. Lett.* 122 127001 (2019).
50. D. C. Freitas et al., Strong enhancement of superconductivity at high pressures within the charge-density-wave states of  $2H$ -TaS<sub>2</sub> and  $2H$ -TaSe<sub>2</sub>. *Phys. Rev. B* 93 184512 (2016).
51. B. Sipoš et al., From Mott state to superconductivity in  $1T$ -TaS<sub>2</sub>. *Nature Mater.* 7, 960 (2008).
52. B. Wang et al., Pressure-induced bulk superconductivity in a layered transition-metal dichalcogenide  $1T$ -tantalum selenium. *Phys. Rev. B* 95, 220501(R) (2017).
53. A. F. Kusmartseva, B. Sipoš, H. Berger, L. Forró, and E. Tutič, Pressure induced superconductivity in pristine  $1T$ -TiSe<sub>2</sub>. *Phys. Rev. Lett.* 103, 236401 (2009).
54. S. Sahoo, U. Dutta, L. Harnagea, A.K. Sood, S. Karmakar, Pressure-induced suppression of charge density wave and emergence of Superconductivity in  $1T$ -VSe<sub>2</sub>. *Phys. Rev. B* 101, 014514 (2020).

55. H. Yao, J. A. Robertson, E.-A. Kim, and S. A. Kivelson, Theory of stripes in quasi-two-dimensional rare-earth tellurides. Phys. Rev. B 74, 245126 (2006).
56. S. Badoux et al., Change of carrier density at the pseudogap critical point of a cuprate superconductor. Nature 531, 210 (2016).

### Figures and Tables

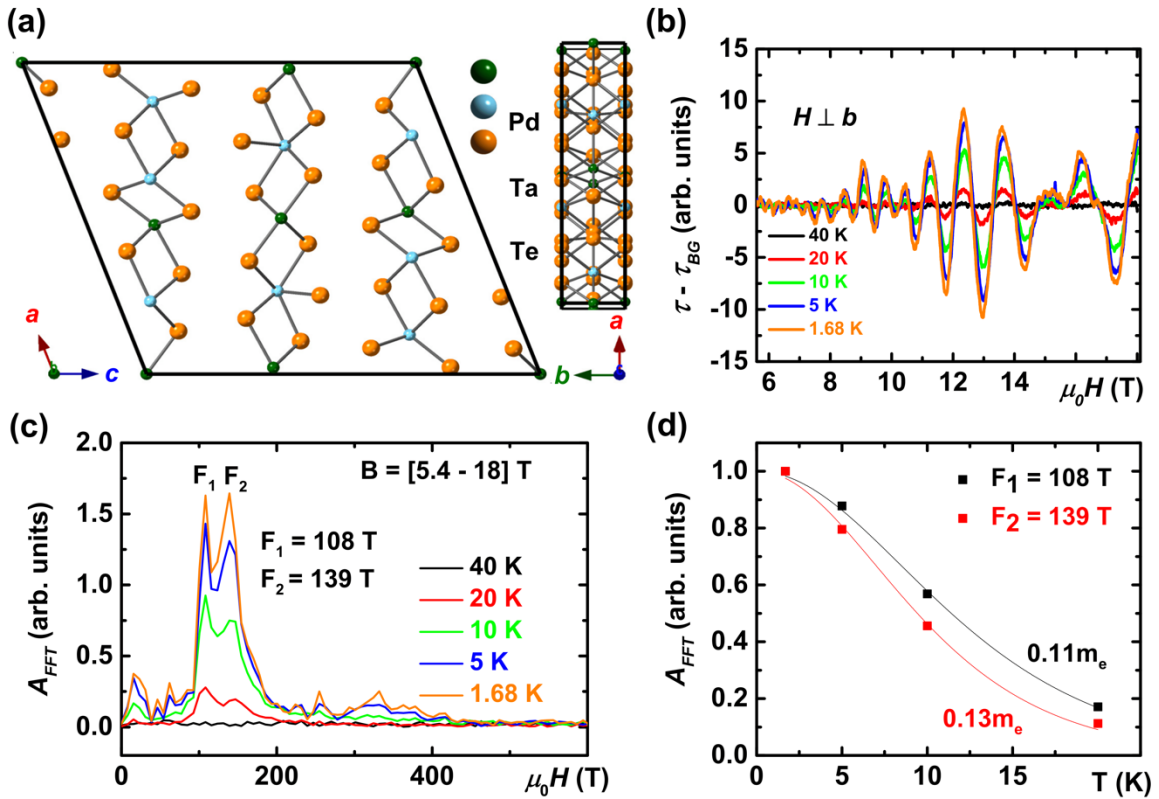


**Figure 1.** (a) Crystal structure of Ta<sub>4</sub>Pd<sub>3</sub>Te<sub>16</sub> along the [010] and [-103] directions in one unit cell. Chains along **b** comprise planes perpendicular to **c**. (b) dHvA oscillation data with polynomial background subtracted at various temperatures measured in an 18 T superconducting magnet. (c) Fourier transform of the data from (b) over a field window of 5.4 to 18 T. (d) Lifshitz-Kosevich fitting of the effective mass.

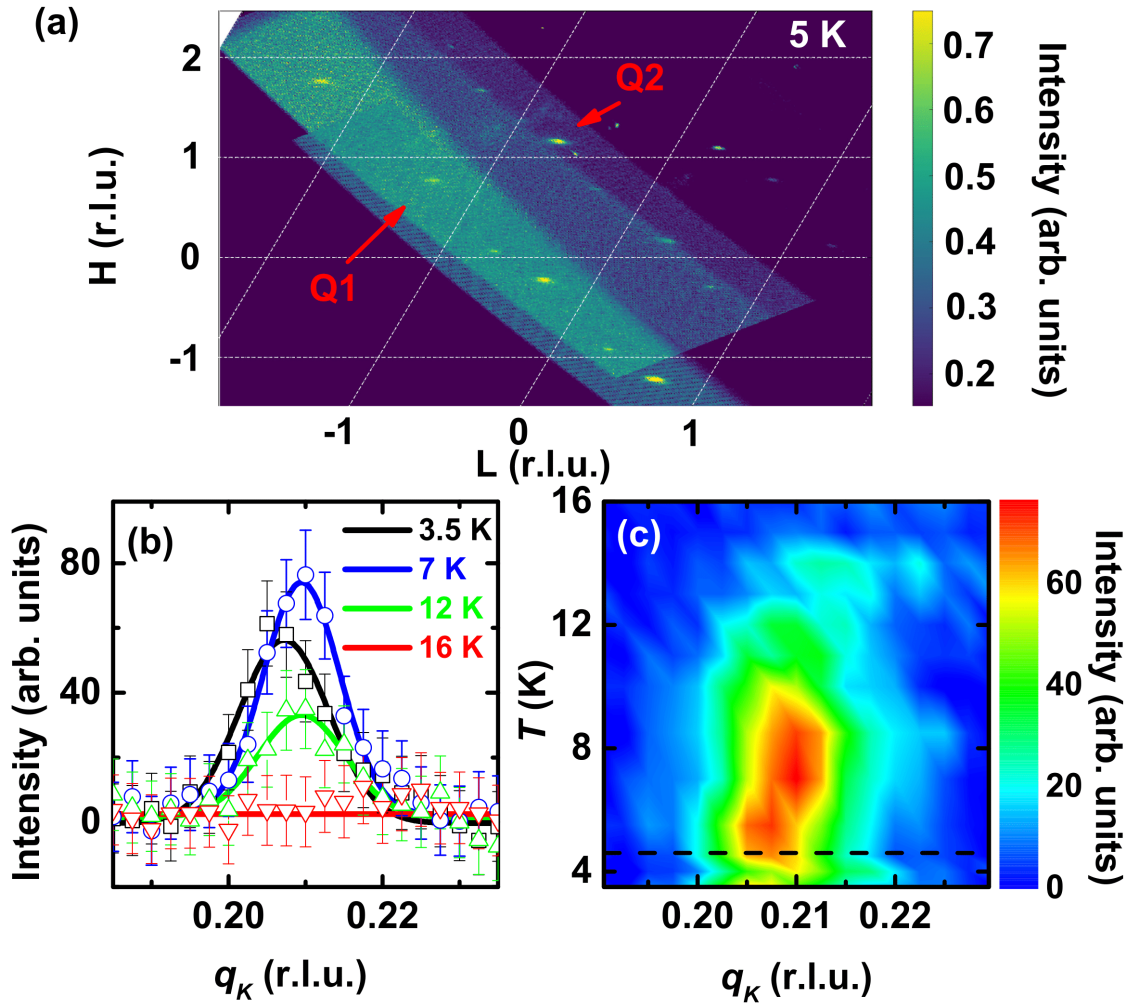


**Figure 2.** (a) 2D cut of the diffraction pattern along the  $H$  and  $L$  directions at  $K=4.21$  for  $T = 5$  K, where  $H$ ,  $K$ , and  $L$  positions are given in reciprocal lattice units (r.l.u.). Two CDW peaks, labeled as Q1 and Q2, appear in all the Brillouin zones covered in the experiment: Q1  $\sim (-0.20, 0.21, -0.30)$  and Q2  $\sim (0.20, 0.21, 0.30)$ . (b) The projected  $(-1, 4, 1) + (-0.20, q_K, -0.30)$  Q1 CDW peak profile along the  $K$  direction for several temperatures, with a 30 K background trace subtracted. Solid lines are Lorentzian fits to data. Error bars correspond to 1 SD. (c) Contour plot of the background-subtracted projected Q1 CDW intensity along the  $K$  direction for temperatures below 20 K. The dashed line indicates the superconducting  $T_c = 4.6$  K (Ref. (17)).

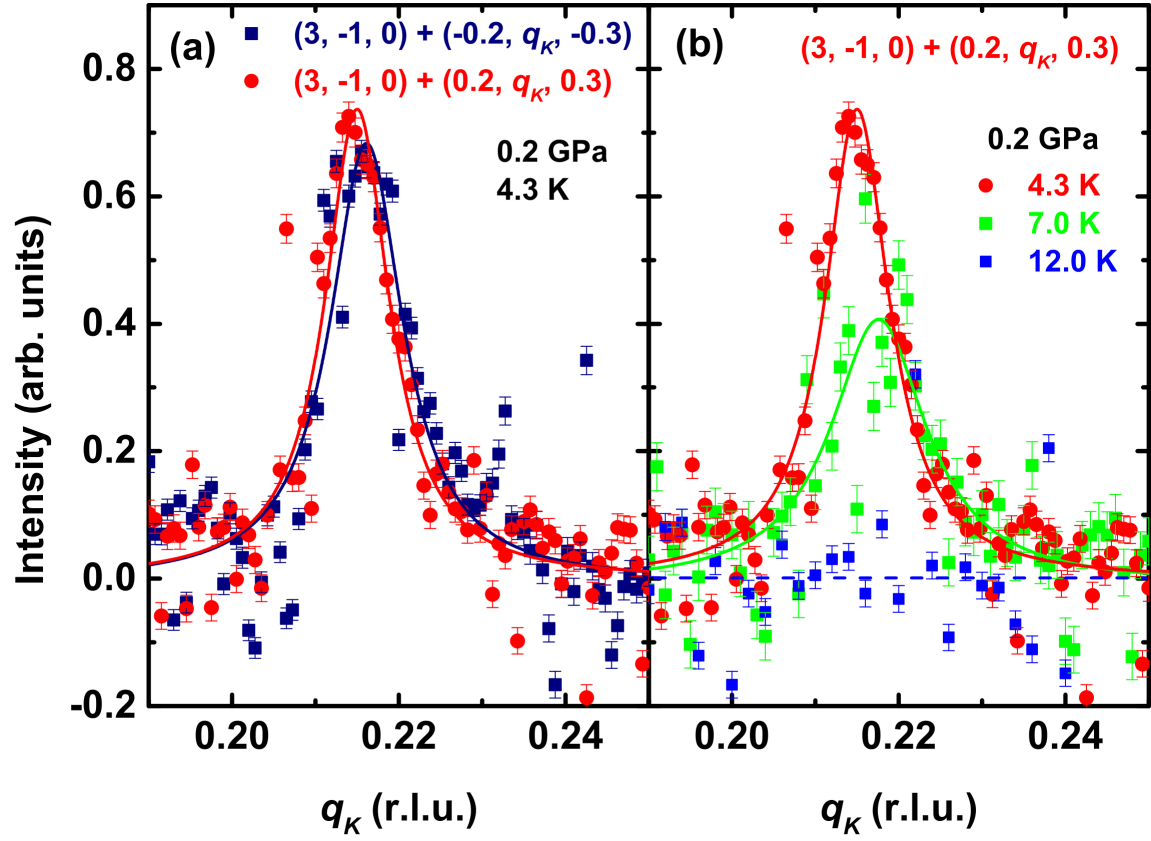


**Figure 3.** (a) The projected Q1 and Q2 CDW peak profiles along the K direction near  $(3, -1, 0)$  at  $T = 4.3$  K and  $P = 0.2$  GPa. (b) The temperature dependence of the projected Q2 CDW peak profile at  $P = 0.2$  GPa. A linear background is subtracted from all the data. Solid lines are Lorentzian fits to the data. The dashed line is a guide to the eye. Error bars correspond to 1 SD.

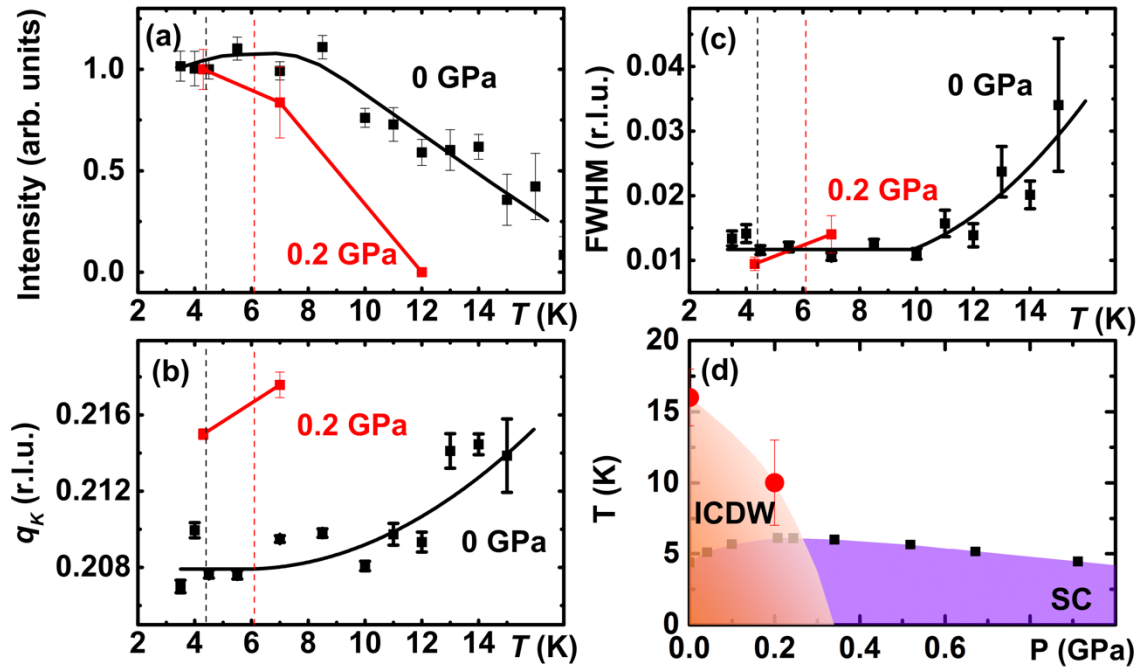


**Figure 4.** The temperature dependence of (a) the normalized peak intensity, (b) the peak position, and (c) the full-width at half-maximum (FWHM) along  $\mathbf{q}_k$  for the Q1 CDW at 0 GPa and Q2 CDW at 0.2 GPa. The peak intensity shown in (a) is normalized to its value at 4.5 K for ambient pressure and its value at 4.3 K for 0.2 GPa. Solid lines are guides to the eye. Black and red dashed lines indicate the superconducting  $T_c$  at ambient pressure and 0.2 GPa [Ref. (17,22)].

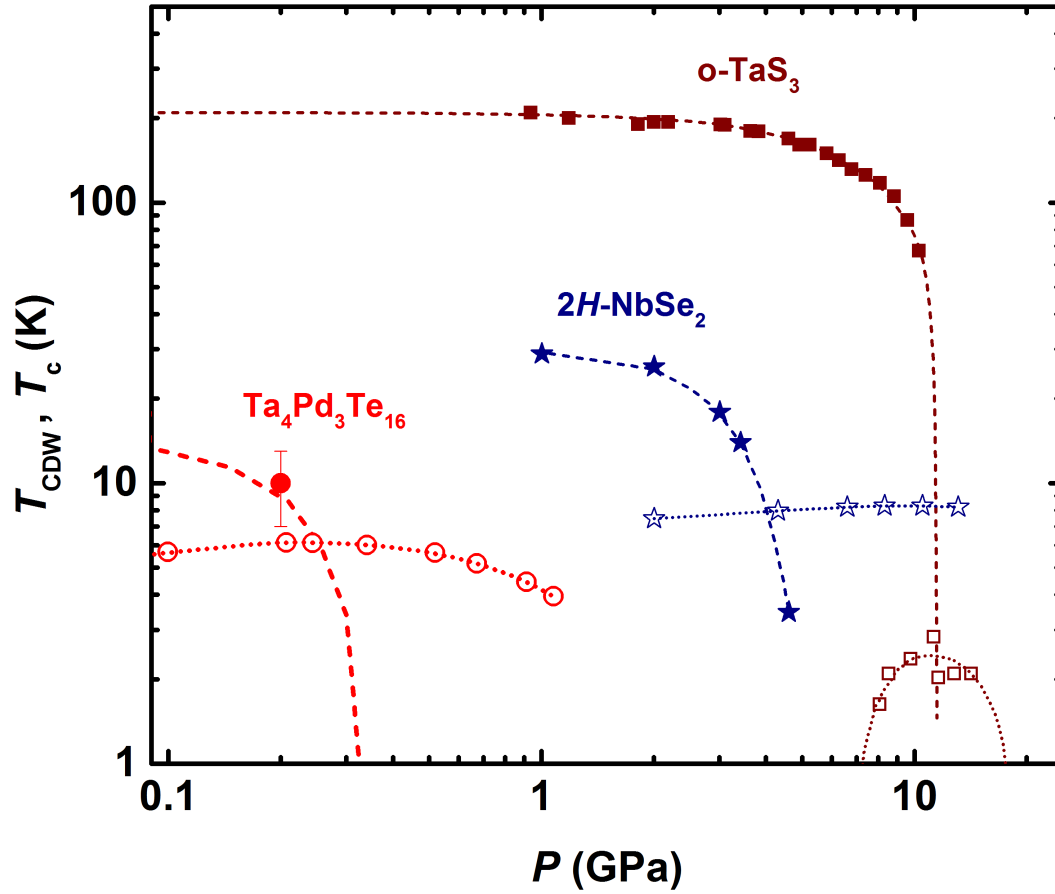


**Figure 5.** Phase diagram of a few selected compounds, as a function of temperature and pressure, showing  $T_{CDW}$  (solid symbols) and  $T_c$  (empty symbols). Our CDW measurements for  $Ta_4Pd_3Te_{16}$  are shown along with  $T_c$  values from Ref. (22). Other compounds:  $2H\text{-NbSe}_2$  (48);  $o\text{-TaS}_3$  (45, 46).

Supplementary Information for

## Direct observation of an incommensurate two-dimensional checkerboard charge density wave in the superconductor $\text{Ta}_4\text{Pd}_3\text{Te}_{16}$

S. J. Kuhn<sup>a,1</sup>, Zhenzhong Shi<sup>a,1</sup>, F. Flicker<sup>b</sup>, T. Helm<sup>c</sup>, J. Lee<sup>d</sup>, William Steinhardt<sup>a</sup>, Sachith Dissanayake<sup>a</sup>, D. Graf<sup>e</sup>, J. Ruff<sup>d</sup>, G. Fabbris<sup>f</sup>, D. Haskel<sup>f</sup>, and S. Haravifard<sup>d,g,2</sup>.

<sup>a</sup>Department of Physics, Duke University, Durham, NC 27708, USA; <sup>b</sup>Rudolph Peierls Centre for Theoretical Physics, University of Oxford, Department of Physics, Clarendon Laboratory, Parks Road, Oxford OX1 3PU, UK; <sup>c</sup>Max Planck Institute for Chemical Physics of Solids, Dresden, Germany; <sup>d</sup>Cornell High Energy Synchrotron Source, Cornell University, Ithaca, NY 14853, USA; <sup>e</sup>National High Magnetic Field Laboratory, Florida State University, Tallahassee, FL 32310, USA; <sup>f</sup>Advanced Photon Source, Argonne National Laboratory, Argonne, IL 60439, USA; <sup>g</sup>Department of Mechanical Engineering & Materials Science, Duke University, Durham, NC 27708, USA

<sup>1</sup> S.K. and Z.S. contributed equally to this work

<sup>2</sup> To whom correspondence should be addressed: S. Haravifard

Email: [haravifard@phy.duke.edu](mailto:haravifard@phy.duke.edu)

**This PDF file includes:**

Figures S1

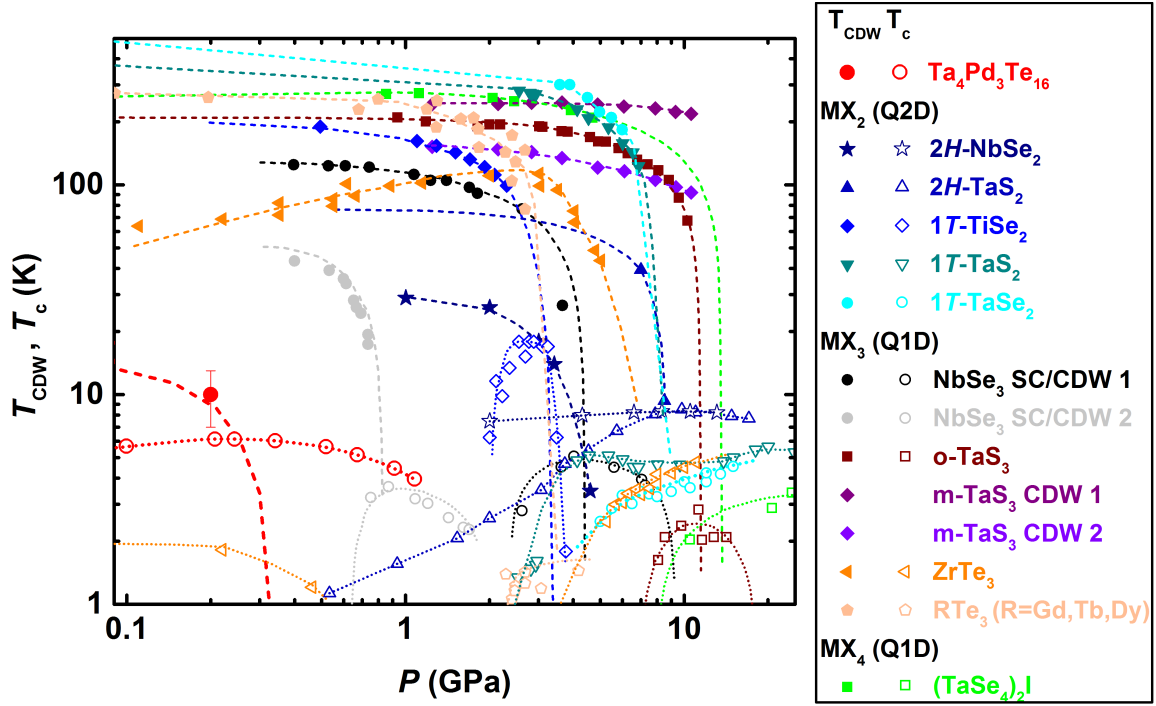


**Fig. S1.** Phase diagram of prototypical compounds, as a function of temperature and pressure, showing  $T_{\text{CDW}}$  (solid symbols) and  $T_c$  (empty symbols). Our CDW measurements for  $\text{Ta}_4\text{Pd}_3\text{Te}_{16}$  are shown along with  $T_c$  values from Ref. (22). Other compounds:  $2H\text{-NbSe}_2$  (48),  $2H\text{-TaS}_2$  (49, 50);  $1T\text{-TaS}_2$  (51);  $1T\text{-TaSe}_2$  (52);  $1T\text{-TiSe}_2$  (53);  $(\text{TaSe}_4)_2\text{I}$  (45, 46);  $o\text{-TaS}_3$  and  $m\text{-TaS}_3$  (45, 46);  $\text{ZrTe}_3$ ,  $\text{GdTe}_3$ ,  $\text{TbTe}_3$ ,  $\text{DyTe}_3$  (47);  $\text{NbSe}_3$  (45, 46).